Localized interface optical phonon modes in a semi-infinite superlattice with a cap layer

2002 J. Phys.: Condens. Matter 14 13761

(http://iopscience.iop.org/0953-8984/14/50/305)

INSTITUTE OF PHYSICS PUBLISHING JOURNAL OF PHYSICS: CONDENSED MATTER

J. Phys.: Condens. Matter **14** (2002) 13761–13775 PII: S0953-8984(02)39475-X

Localized interface optical phonon modes in a semi-infinite superlattice with a cap layer

Ke-Qiu Chen[1], **Wenhui Duan**[1], **Jian Wu**[1], **Bing-Lin Gu**[1] **and Ben-Yuan Gu**[2,3]

[1] Department of Physics, Tsinghua University, Beijing 100084, China
[2] CCAST(World Laboratory), PO Box 8730, Beijing 100080, China
[3] Institute of Physics, Chinese Academy of Sciences, PO Box 603, Beijing 100080, China

E-mail: keqiuchen@mail.tsinghua.edu.cn

Received 15 July 2002
Published 6 December 2002
Online at stacks.iop.org/JPhysCM/14/13761

Abstract

We investigate the existence and characteristics of the localized interface optical phonon modes (IOPMs) in a semi-infinite AlAs–GaAs superlattice with a cap layer consisting of ternary mixed crystal $Al_xGa_{1-x}As$ in the dielectric continuum approximation. We find that the introduction of two-mode behaviour of the ternary mixed crystal of the cap layer or the semi-infinite uniform dielectric medium leads to rich and varied localized mode spectra with interesting features. Moreover, it is also found that the localized IOPMs are sensitive to the concentration x, the thickness of the cap layer and the type of semi-infinite uniform dielectric medium. A brief analysis of these results is given. It is expected that the localized IOPMs can be artificially controlled by adjusting the parameters of the proposed micro-structures.

(Some figures in this article are in colour only in the electronic version)

1. Introduction

Progress in microfabrication techniques enables us to produce various kinds of superlattice (SL) from a variety of materials including semiconductors, metals and magnetically ordered materials. The thickness of each layer in the SLs can also be controlled with considerable accuracy. Physical properties of such a structure are quite distinct from either constituent, and depend on the material and relative widths of constituent layers in a unit cell as well as periodicity. The optical vibrational properties in these structures have been extensively investigated both theoretically [1–10] and experimentally [11–17] during the past two decades. The interface optical-phonon modes (IOPMs) have been found to play a dominant role in electron–phonon interactions in quantum wells and SLs [18–23]. Both macroscopic and microscopic approaches to optical phonon modes have been applied in theoretical treatments [1, 4], and the dispersion relation of the IOPMs can be analysed within the framework

of dielectric continuum theory [1, 13]. Now, it is well known that for a perfect AlAs–GaAs SL, its bands of IOPMs are composed of a pair of higher-energy AlAs-like and a pair of lower-energy GaAs-like bands in a Brillouin zone. Each pair of bands is always separated by a gap, while the gap disappears when the width of layer a is equal to that of layer b.

There is significant interest in the properties of localized optical vibrational modes inside the frequency minigaps of a superlattice in the presence of inhomogeneities such as surfaces, interfaces or defect layers in recent years. Camley and Mills [1] studied the surface phonon polaritons in a two-layer semi-infinite superlattice composed of Al and insulator layers. The dispersion curves of surface phonons in a finite superlattice were revealed by Johnson *et al* [24], Nkoma [25] and Liu *et al* [26]. The dispersion curves of the surface phonon in a semi-infinite GaAs–AlAs superlattice with a topmost layer changing in thickness were reported by Streight and Mills [27], and extended to the finite superlattice by Tsuruoka *et al* [28]. Surface phonon polaritons have also been investigated within three-layer SLs [29]. Recently, the properties of the localized electromagnetic modes in a semi-infinite SL with a cap layer [30] and in a finite superlattice [31], and of localized polariton modes in periodic Bragg multiple-quantum-well structures [32] have also been explored. The authors have investigated the localized IOPMs in GaAs/AlAs SL with structural defect layers [33] and with ternary mixed crystal defect layers [34]. They found that for the cases with structural defect layers [33] the localized IOPMs always appear in pairs inside each minigap and possess either symmetric or antisymmetric behaviours with respect to the centre of the defect layer, corresponding to longitudinal and transverse vibrations, respectively. However, for the cases with ternary mixed crystal defect layers $Al_xGa_{1-x}As$ [34], there are three localized IOPMs in each minigap for certain structural parameters and concentrations x; two of them are antisymmetric and display interesting features significantly different from those in the structure with a binary crystal defect layer, while the other one is symmetric and exhibits similar behaviour to that in the structure with a binary crystal defect layer.

In the present paper we investigate the localized IOPMs in the structure where a cap layer consisting of ternary mixed crystal $Al_xGa_{1-x}As$ is embedded between a semi-infinite GaAs–AlAs superlattice and the frequency-dependent (or frequency-independent) semi-infinite uniform dielectric medium $Al_yGa_{1-y}As$. As well known, for long waves, the superlattice behaves as a homogeneous, anisotropic crystal [13]. Then one may inquire if there exist new features for the localized IOPMs in the present structure in comparison with the structure where an inhomogeneous layer is embedded between two coupling semi-infinite SLs, as studied in [34, 35]. We will indicate that the present structure does have some new and very interesting features. Moreover, we will also examine the effects of a ternary mixed crystal cap layer on the localized IOPMs (or surface modes) in a semi-infinite SL with (or without) a frequency-independent semi-infinite uniform dielectric medium. Our results show that the introduction of the two-mode behaviour of the ternary mixed crystal can lead to a dramatic change of the localized IOPMs (or surface modes) in the structures considered here.

This paper is organized as follows. In section 2, we give a brief description of the model and the necessary formulae used in calculations. The numerical results are presented in section 3 with analyses. Finally, we summarize our results in section 4.

2. Model and formulae

We consider a structure such as shown in figure 1, in which a cap layer labelled as d (material $Al_xGa_{1-x}As$) with a thickness of W_d is embedded between a semi-infinite SL with the unit cell composed of a (GaAs) and b (AlAs) materials and a semi-infinite frequency-dependent uniform dielectric medium ($Al_yGa_{1-y}As$) labelled as c. The dielectric constants of materials

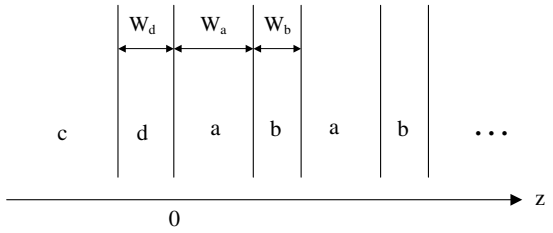

Figure 1. Schematic diagram of a semi-infinite superlattice with a cap layer d attached to semi-infinite uniform dielectric medium c. W_d, W_a and W_b denote the thicknesses of the cap layer and the two constituent layers of the unit cell of the semi-infinite SL, respectively.

a, b, c and d are $\epsilon_a(\omega)$, $\epsilon_b(\omega)$, $\epsilon_c(\omega)$ and $\epsilon_d(\omega)$, respectively. The thicknesses of constituent layers a and b are W_a and W_b, respectively, and the period of the semi-infinite superlattice is $W = W_a + W_b$.

In this paper, we adopt the dielectric continuum model to investigate localized IOPMs. It is necessary to note that this model is valid in the long-wavelength limit in bulk material. However, this model is still a rather good approximation in several mini-Brillouin-zone scales of wavenumber q for the SL structure due to the period of the SL being much larger than the lattice constant of the bulk materials. This conclusion has been confirmed by microscopic calculations [4] and Raman experiments [12].

In treatment of IOPMs, we shall ignore the effects of retardation; then the macroscopic electrostatic potential $\phi(\boldsymbol{r})$ obeys Laplace's equation:

$$\nabla^2\phi(\boldsymbol{r}) = 0. \tag{1}$$

As the translational invariance of the system is retained in the two directions parallel to the interface, and thus it is assumed that each material is isotropic without loss of generality, the electrostatic potential has the form of $\phi(\boldsymbol{r}) = \phi(z)\mathrm{e}^{\mathrm{i}q_\parallel y}$, where $q_\parallel$ is the wavevector lying on the (x, y) plane and is the same for all materials in the structure. Then we can write down the electrostatic potential in an individual region. For a semi-infinite superlattice, the electrostatic potential in the slab of material a for the region $nW < z < nW + W_a$ is (n is an integer number)

$$\Phi(z) = \mathrm{e}^{-q_z nW}(A_+\mathrm{e}^{q_\parallel(z-nW)} + A_-\mathrm{e}^{-q_\parallel(z-nW)}), \tag{2}$$

while in slab b for the region $nW + W_a < (n+1)W$ we have

$$\Phi(z) = \mathrm{e}^{-q_z nW}(B_+\mathrm{e}^{q_\parallel(z-nW-W_a)} + B_-\mathrm{e}^{-q_\parallel(z-nW-W_a)}), \tag{3}$$

where q_z is the attenuation constant and its real part should be positive for the localized IOPMs. In the region $-W_d < z < 0$ we have

$$\Phi(z) = D_+\mathrm{e}^{q_\parallel z} + D_-\mathrm{e}^{-q_\parallel z}, \tag{4}$$

and in the region $z < -W_d$ we have

$$\Phi(z) = C\mathrm{e}^{q_\parallel(z+W_d)}. \tag{5}$$

By applying the boundary conditions that the electrostatic potential, along with the normal component of the displacement field $\boldsymbol{D}[\boldsymbol{D} = \epsilon\boldsymbol{E}]$, should be continuous at each interface, one can interrelate various coefficients appearing in the above-mentioned expressions and derive an implicit dispersion relation for the localized IOPMs:

$$c_1c_2(f_1^2\mathrm{e}^{-q_\parallel W_a} + f_2^2\mathrm{e}^{q_\parallel W_a})\sinh(q_\parallel W_b) = f_1f_2\{c_1^2\sinh(q_\parallel W) + c_2^2\sinh[q_\parallel(W_b - W_a)]\}, \tag{6}$$

where

$$c_1 = 1 + \frac{\epsilon_a}{\epsilon_b}, \tag{7}$$

$$c_2 = 1 - \frac{\epsilon_a}{\epsilon_b}, \tag{8}$$

$$f_1 = \left(1 - \frac{\epsilon_a}{\epsilon_c}\right)\cosh(q_\parallel W_d) + \left(\frac{\epsilon_d}{\epsilon_c} - \frac{\epsilon_a}{\epsilon_d}\right)\sinh(q_\parallel W_d), \tag{9}$$

and

$$f_2 = \left(1 + \frac{\epsilon_a}{\epsilon_c}\right)\cosh(q_\parallel W_d) + \left(\frac{\epsilon_d}{\epsilon_c} + \frac{\epsilon_a}{\epsilon_d}\right)\sinh(q_\parallel W_d). \tag{10}$$

The attenuation constant q_z is determined by an equation which is identical to the expression appropriate to the perfect superlattice,

$$\cosh(q_z W) = \cosh(q_\parallel W_a)\cosh(q_\parallel W_b) + \frac{1}{2}\left(\frac{\epsilon_a}{\epsilon_b} + \frac{\epsilon_b}{\epsilon_a}\right)\sinh(q_\parallel W_a)\sinh(q_\parallel W_b). \tag{11}$$

For the binary crystal AlAs or GaAs, the dielectric functions are expressed in the form

$$\epsilon_i(\omega) = \epsilon_{\infty i}\frac{(\omega^2 - \omega_{LOi}^2)}{(\omega^2 - \omega_{TOi}^2)} \qquad (i = a, b), \tag{12}$$

where i corresponds to material a (GaAs) or b (AlAs), $\omega_{LOi}(\omega_{TOi})$ is the longitudinal(transverse) optical-phonon frequency of the binary crystal and $\epsilon_{\infty i}$ the optical dielectric constant of material i $(i = a, b)$; while for the ternary mixed crystal $Al_xGa_{1-x}As$, the long-wavelength optical phonons exhibit the two-mode behaviour, and the dielectric function has the form [35]

$$\epsilon(\omega) = \epsilon_\infty\frac{(\omega^2 - \omega_{LOa}^2)(\omega^2 - \omega_{LOb}^2)}{(\omega^2 - \omega_{TOa}^2)(\omega^2 - \omega_{TOb}^2)}, \tag{13}$$

where ϵ_∞ represents the dielectric constant of $Al_xGa_{1-x}As$. The two-mode behaviour of the ternary mixed crystal in equation (13) is distinguished by subscripts a and b which respectively stand for GaAs-like and AlAs-like modes. Here, it should be particularly noted that in numerical studies of the dispersion relations of the localized IOPMs one seeks the roots of equation (6). Once a root is found, it is necessary to insure that the real part of the attenuation constant q_z determined by equation (11) is positive (namely $\mathrm{Re}(q_z) > 0$) for the localized IOPMs. In the following section, we present the results of numerical calculations of the dispersion relation of the localized IOPMs for the structure shown in figure 1. In the calculations, we employ those values of dielectric constants and phonon frequencies of GaAs, AlAs and $Al_xGa_{1-x}As$ referred to [9] and [36]: $\epsilon_\infty(\mathrm{GaAs}) = 10.89$ and $\epsilon_\infty(\mathrm{AlAs}) = 8.16$, $\omega_{LO}(\mathrm{GaAs}) = 55.045$, $\omega_{TO}(\mathrm{GaAs}) = 50.550$, $\omega_{LO}(\mathrm{AlAs}) = 76.061$ and $\omega_{TO}(\mathrm{AlAs}) = 68.150$ THz; while $Al_xGa_{1-x}As$ has both AlAs-like and GaAs-like modes:

$$\omega_{LO}(\mathrm{GaAs\text{-}like}) = 55.0450 - 9.9461x + 2.7181x^2, \tag{14}$$

$$\omega_{TO}(\mathrm{GaAs\text{-}like}) = 50.5503 - 0.9718x - 1.7614x^2, \tag{15}$$

$$\omega_{LO}(\mathrm{AlAs\text{-}like}) = 67.7699 + 13.3323x - 5.0414x^2, \tag{16}$$

$$\omega_{TO}(\mathrm{AlAs\text{-}like}) = 67.7699 + 0.8352x - 0.4555x^2. \tag{17}$$

Note that the phonon frequencies cited above correspond to the case of $q = 0$. The value of the dielectric constant of $Al_xGa_{1-x}As$ is evaluated by

$$\epsilon_\infty(Al_xGa_{1-x}As) = 10.89 - 2.73x. \tag{18}$$

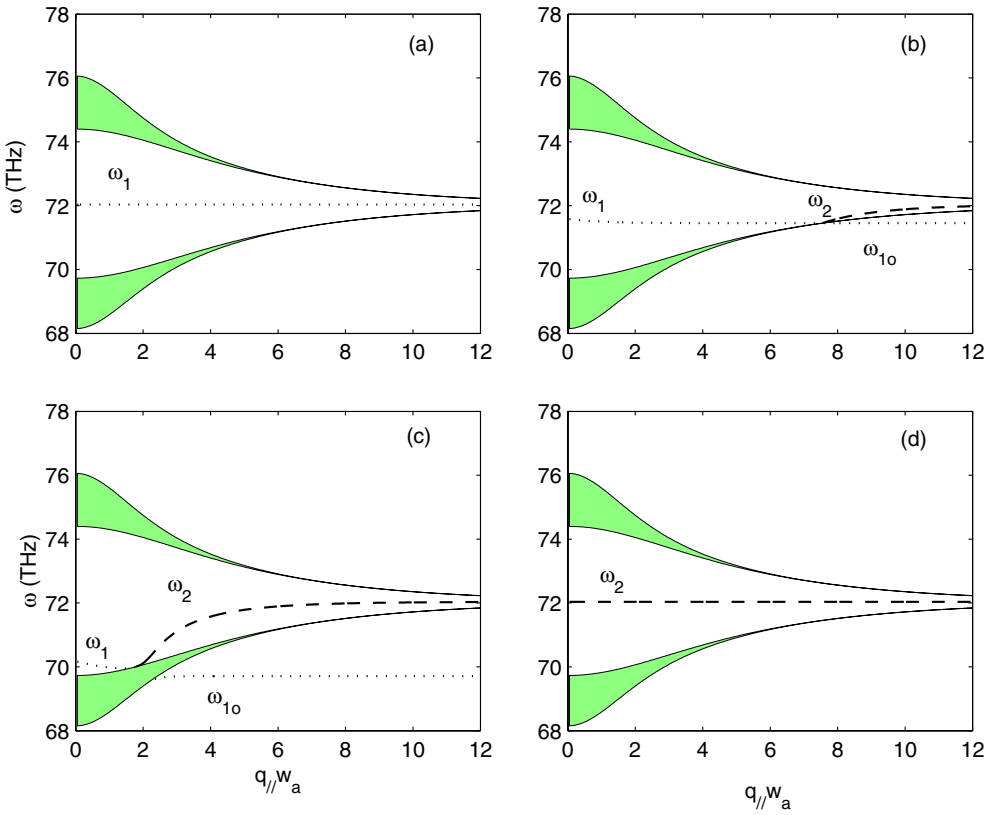

Figure 2. Calculated frequencies of the AlAs-like localized IOPMs as a function of the transverse wavenumber $q_\parallel$ for different concentrations y of the semi-infinite uniform dielectric medium. (a)–(d) correspond to $y = 1$, 0.7, 0.3 and 0.0, respectively. ω_1, ω_2 and ω_{1o} represent the localized IOPMs lying inside the minigap and outside the bulk bands, respectively. The shaded areas denote the bulk bands of the SL, and the region between two bulk bands represents the minigap.

3. Numerical results and analyses

We first display the calculated frequency dependence of the AlAs- and GaAs-like localized IOPMs lying inside the minigap, below and above the bulk bands on the transverse wavenumber $q_\parallel$ for different concentrations y of semi-infinite uniform dielectric medium c in figures 2 (for the AlAs-like) and 3 (for the GaAs-like): (a)–(d) correspond to $y = 1, 0.7, 0.3$ and 0.0, respectively. Here, we take $W_a = 20$ nm, $W_b = 5$ nm and $W_d = 0$. Indeed, for these parameters, the structure is recovered to a semi-infinite SL attached to a semi-infinite uniform dielectric medium c. From figure 2(a), for $y = 1$, it is clearly seen that there is one branch of localized IOPM labelled as ω_1 lying in the middle of the AlAs-like minigap, and this localized mode is independent of the transverse wavenumber $q_\parallel$. With the decrease of the concentration y, the localized mode ω_1 shifts towards the lower-frequency region and finally merges into the lower bulk band (see figure 2(d)); and at the same time one branch of the new localized mode ω_2 is extracted from the bulk band, as shown in figure 2(b). Moreover, one branch of the localized mode labelled as ω_{1o} appears below the lower bulk band. Localized mode ω_{1o} looks like the elongation of the ω_1 branch, and has similar localization behaviours as the ω_1 branch which will be seen subsequently, so we mark it in the same style of lines as the ω_1

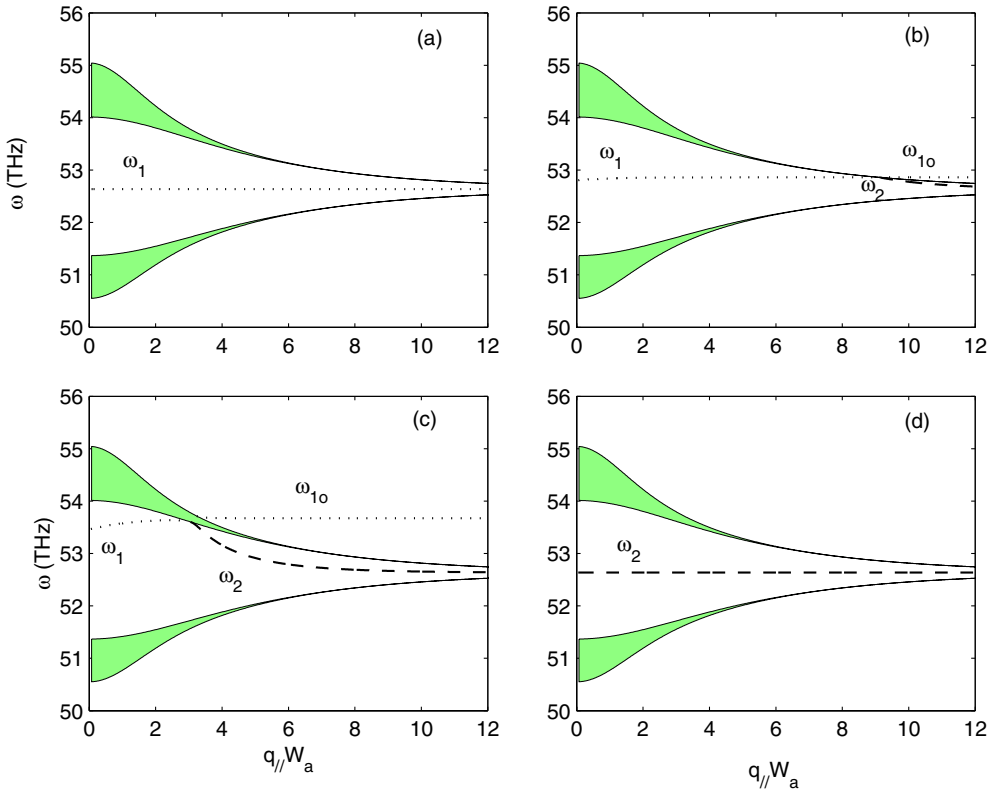

Figure 3. Calculated frequencies of the GaAs-like localized IOPMs as a function of the transverse wavenumber $q_\parallel$ for different concentrations y of the semi-infinite uniform dielectric medium. (a)–(d) correspond to $y = 1$, 0.6, 0.3 and 0.0, respectively. Explanations for all curves are the same as for figure 2.

mode and assign it to be ω_{1o}. When further decreasing y, all these three localized modes shift towards the left-hand region on the abscissa. When $y = 0$, only ω_2 survives, lying in the middle of the minigap. For the case of GaAs-like localized IOPMs, the corresponding results are displayed in figure 3; similar features are observed. But all the localized modes now shift towards the higher-frequency region and ω_{1o} is located above the bulk band. Here, it is noted that the attenuation constants q_z of the localized modes inside the minigap are purely real and positive, and the q_z of the localized modes below and above the bulk bands are associated with $q_z W = q_0 + \mathrm{i}\pi$, where q_0 is positive. For two special cases, where the material of the semi-infinite dielectric medium becomes pure AlAs or GaAs (namely, y is taken as unity or zero), from equations (5)–(10), one can derive the formula of $\epsilon_a(\omega) = \pm\epsilon_b(\omega)$, which determines the dispersion curves of the localized modes. Consequently, the frequencies of the localized modes have nothing to do with the transverse wavenumber $q_\parallel$, the thicknesses of the cap layer or the constituent layers. Thus there is only one localized IOPM surviving in the middle of the minigap, as shown in figures 2(a) and (d) (or figures 3(a) and (d)). It is worth mentioning in particular that the two-mode behaviour of the ternary mixed crystal semi-infinite dielectric medium c leads to the appearance of new localized IOPMs.

In figure 4, we map out the modulus of the macroscopic electrostatic potential associated with AlAs-like localized modes: (a) the ω_1 mode for $y = 1.0$ at $q_\parallel W = 1$; (b) the ω_1 mode for

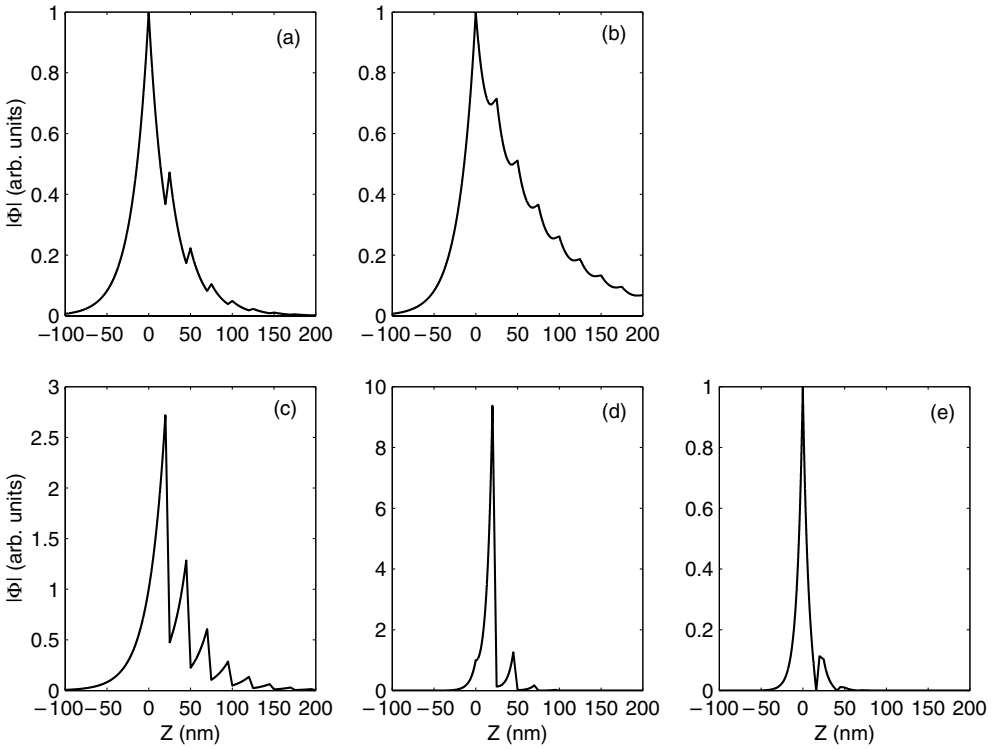

Figure 4. Modulus of the electrostatic potential of the AlAs-like localized IOPMs for the same structural parameters as in figure 2. (a) ω_1 mode for $y = 1.0$ at $q_\parallel W = 1$; (b) ω_1 mode for $y = 0.3$ at $q_\parallel W = 1$; (c) ω_2 mode for $y = 0.0$ at $q_\parallel W = 1$; (d) ω_2 mode for $y = 0.3$ at $q_\parallel W = 3$ and (e) ω_{1o} mode for $y = 0.3$ at $q_\parallel W = 3$.

$y = 0.3$ at $q_\parallel W = 1$; (c) the ω_2 mode for $y = 0.0$ at $q_\parallel W = 1$; (d) the ω_2 mode for $y = 0.3$ at $q_\parallel W = 3$ and (e) the ω_{1o} mode for $y = 0.3$ at $q_\parallel W = 3$. $\Phi(z)$ is not normalized. From figures 4(a) and (b), we find that the ω_1 mode for different y is localized in the vicinity of the interface at $z = 0$ and it exhibits similar behaviour, but its localization degree is different for different y. From figures 4(c) and (d), it is clearly seen that the ω_2 branch is localized in the vicinity of the interface at $z = 20$ nm (namely the first GaAs–AlAs interface of a semi-infinite SL). However, the modulus of the electrostatic potential of ω_2 for $y = 0.3$ (see figure 4(d)) only has a small peak beside the strong main peak, different from that with one main peak and several side-lobe peaks for $y = 0$ (see figure 4(c)). The ω_{1o} mode is also localized in the vicinity of $z = 0$, and has similar localization features to those of ω_1 in spite of it exhibiting much more localization than the ω_1 mode, comparing figure 4(e) with (a) or (b). This is also one reason we label it as ω_{1o}. It is interesting to point out that the modulus of the macroscopic electrostatic potential of the localized IOPMs exhibits an oscillatory decay behaviour in the semi-infinite SL, and all the peaks and valleys in the curves are located at the interfaces, which is very different from the results reported in [33] in which the positions of all the peaks and valleys of the modulus of the macroscopic electrostatic potential of the localized IOPMs correspond to the interface and the bisectors of slabs, respectively. This may be attributed to the fact that the structure considered here is asymmetric. It is also the reason why the present localized IOPMs do not couple into an odd or even parity.

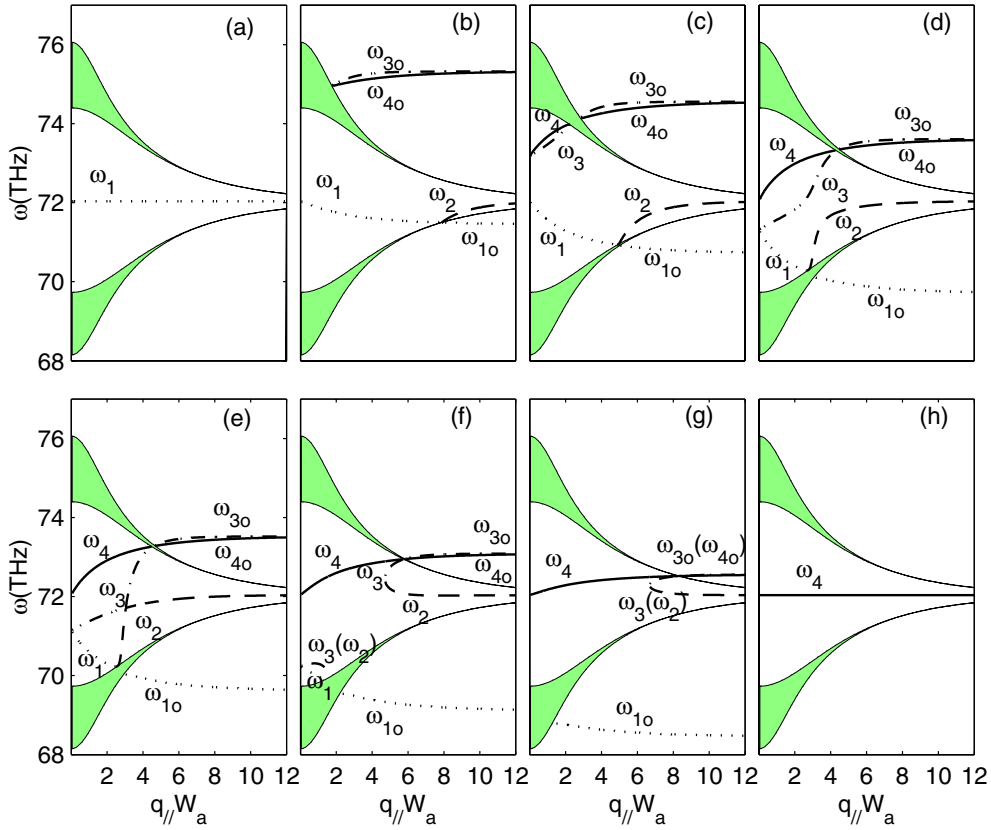

Figure 5. Calculated frequencies of the AlAs-like localized IOPMs as a function of the transverse wavenumber $q_{\|}$ for different concentrations x of the cap layer. (a)–(h) correspond to $x = 1, 0.7, 0.5, 0.3, 0.2833, 0.2, 0.1$ and 0.0, respectively. The dotted, dashed, dot–dashed and solid curves labelled as ω_1, ω_2, ω_3 and ω_4, respectively, represent the localized IOPMs lying inside the minigap. ω_{1o} represents the localized modes lying below the lower bulk bands; ω_{3o} and ω_{4o} denote the localized modes lying above the upper bulk band. The shaded areas indicate the bulk bands of the SL, and the region between two bulk bands represents the minigap.

Dispersion curves of the AlAs-like localized IOPMs are shown in figure 5 for the case where the concentration y of the semi-infinite uniform dielectric medium c is fixed to unity, and the concentration x of the cap layer d is varied from unity to zero: (a)–(h) correspond to $x = 1.0, 0.7, 0.5, 0.3, 0.2833, 0.2, 0.1$ and 0.0, respectively. Here, we take $W_a = 20$ nm, $W_b = 5$ nm and $W_d = 3$ nm. When the cap layer is AlAs ($x = 1$, see figure 5(a)) or GaAs ($x = 0$, see figure 5(h)), only one branch of the localized mode exists in the middle of the minigap regardless of the width of the cap layer. However, when the cap layer is ternary mixed crystal, namely $0 < x < 1$ (see figures 5(b)–(g)), several branches of the localized modes can arise out inside the minigap, below and above the bulk bands, and they display interesting features. From figures 5(a)–(h), we can clearly observe the evolution of the localized modes with the decrease of the concentration x of the cap layer. There are at most four branches of the localized modes labelled as ω_1, ω_2, ω_3 and ω_4, respectively, existing inside the minigap. Their attenuation constants q_z are purely real. Moreover, there exists one branch of the localized mode labelled as ω_{1o} below the lower bulk band and two branches of localized modes labelled

as ω_{3o} and ω_{4o} above the upper bulk bands. They look like the elongation of ω_1, ω_3 and ω_4, respectively, and their attenuation constants q_z are associated with $q_z W = q_0 + i\pi$ ($q_0 > 0$). It is interesting to note from figures 5(c)–(g) that, with the decrease of the concentration x of the cap layer, ω_2 and ω_3 branches gradually approach each other. It looks as if there is an attraction interaction between the ω_2 mode and the ω_3 mode. When x is about 0.2833, both the ω_2 mode and the ω_3 mode become degenerate at a certain transverse wavenumber $q_\parallel$ (see figure 5(e)). This behaviour seems to be analogous to the coupling between the quasi-longitudinal and quasi-transverse acoustic modes having propagation directions oblique to the interface in the SL presented in [37, 38]. Both ω_2 and ω_3 can couple together when they meet each other, which indicates that they have some of the same orientation of the polarization, namely they contain some of the same longitudinal or transverse lattice vibration characters. The mixing of the polarization between these modes leads to the coupling. With further increase of x, the dispersion curves of the ω_2 mode and the ω_3 mode are divided into two parts; their left-hand part or their right-hand part is joined together and it is difficult to distinguish them now. The left-hand part or the right-hand part of the ω_2 mode and the ω_3 mode shifts respectively towards the left- or right-hand region with the decrease of x; and finally both the ω_2 mode and the ω_3 mode disappear. This behaviour appears somewhat suspicious in view of the conservation of total number of localized modes for every value of the wavevector $q_\parallel$. We give an explanation for this as follows. The formation of the bulk bands in the SL results from the periodicity coupling between two adjacent dielectric layers, while for an SL with inhomogeneous layers such as surface, interface or defect layers the periodic coupling is locally broken down around the inhomogeneous layer of the SL. The periodicity-broken coupling leads to the appearance of the new splitting levels. Some of them may lie within the bulk bands and develop into the delocalized scattering modes, and the rest of them reside in the minigaps or below and above the bulk bands, and become localized modes. Though the conservation of the total number of localized modes is broken, the conservation of the total number of all splitting levels including both the delocalized scattering modes and localized modes is still kept for every value of the wavevector $q_\parallel$. Consequently, these results may be understood from physical viewpoints. Figure 5 clearly shows that all the localized modes sensitively depend on the concentration x of the cap layer. The influence of transverse wavenumber $q_\parallel$ on localized modes is also evident except for two special cases presented in figures 5(a) and (h). For these two special cases, interpretations of the dispersion curve have been addressed above. Here, it should be noted that we have also calculated the modulus of the macroscopic electrostatic potential of all localized modes (the results are not plotted here), it is found that ω_{1o}, ω_{3o} and ω_{4o} have similar localization behaviours to those of ω_1, ω_3 and ω_4, respectively. For GaAs-like localized IOPMs, the obtained results are depicted in figure 6; similar features are observed. However, the frequency positions of localized IOPMs are just reversed in sequence.

To further examine the influence of the coupling among the cap layer, semi-infinite medium and semi-infinite SL on the localized IOPMs, in figure 7 we present the dispersion curves of the AlAs-like localized IOPMs for the structure where a ternary mixed crystal cap layer $Al_xGa_{1-x}As$ is embedded between a semi-infinite SL and a frequency-independent semi-infinite uniform medium c such as vacuum or insulators. Here, we assume that the semi-infinite uniform medium c consists of SiO_2 with dielectric constant $\epsilon = 3.7$. Figures 7(a)–(h) correspond to $x = 1.0, 0.7, 0.6, 0.532, 0.4, 0.3, 0.2$ and 0.0, respectively. Here, we take $W_a = 20$ nm, $W_b = 5$ nm and $W_d = 3$ nm. When the cap layer is AlAs ($x = 1$, see figure 7(a)), there exist two branches of the localized IOPMs: one (ω_1) lies in the minigap and another one (ω_2) lies above the upper bulk band, and both of them are varied with the transverse wavenumber $q_\parallel$. However, when the cap layer is GaAs ($x = 0$, see figure 7(h)), only one branch (ω_2) of the localized IOPM exists in the minigap for certain structural parameters. With the

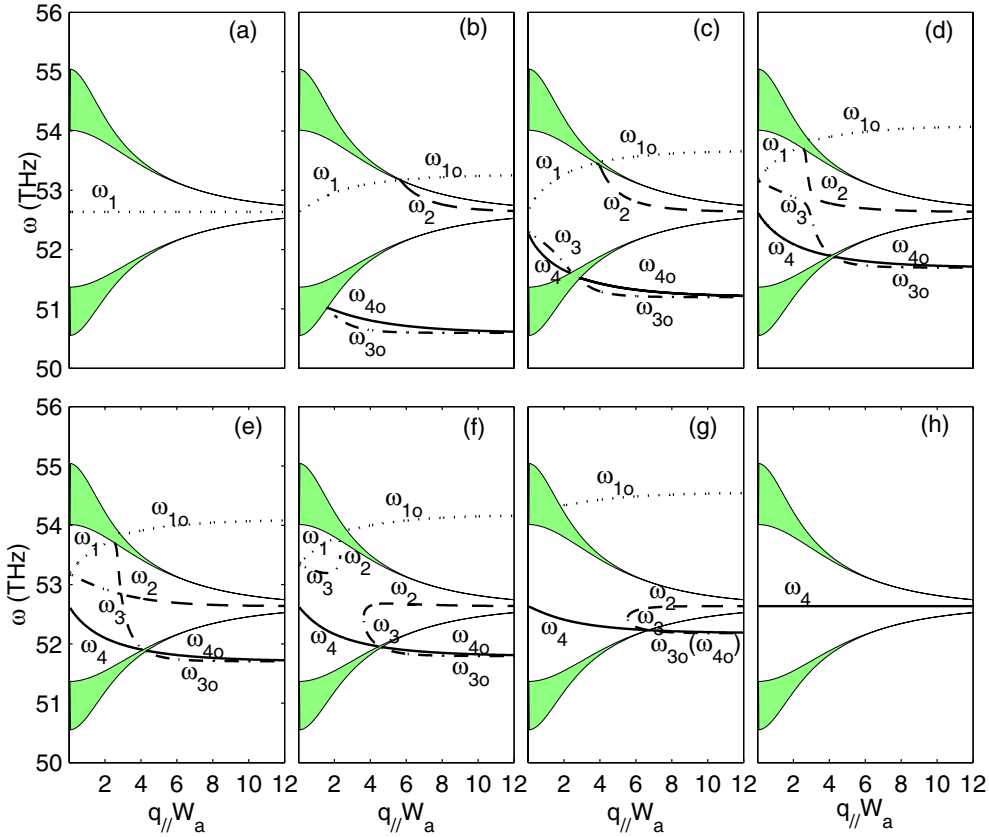

Figure 6. Calculated frequencies of the GaAs-like localized IOPMs as a function of the transverse wavenumber $q_{\|}$ for different concentrations x of the cap layer. (a)–(h) correspond to $x = 1$, 0.42, 0.3, 0.2, 0.1979, 0.18, 0.1 and 0.0, respectively. The dotted, dashed, dot–dashed and solid curves labelled as ω_1, ω_2, ω_3 and ω_4, respectively, represent the localized IOPMs lying inside the minigap. ω_{1o} represents the localized modes lying above the upper bulk bands; ω_{3o} and ω_{4o} denote the localized modes lying below the lower bulk bands. The shaded areas denote the bulk bands of SL, and the region between the two bulk bands represents the minigap.

introduction of the two-mode behaviours of the ternary mixed crystal cap layer, new localized IOPMs now appear in the minigap, above and below the bulk bands. It is clearly seen from figures 7(b)–(g) that the localized modes are varied with the concentration x of the cap layer and the transverse wavenumber $q_{\|}$. With the decrease of the concentration x, the ω_1 branch in the minigap shifts towards the higher-frequency region; meanwhile, ω_2 and ω_3 branches in the minigap as well as ω_{2o} and ω_{3o} (above the bulk band) shift towards the low-frequency region. When x is about 0.532 (see figure 7(d)), both ω_1 and ω_2 modes degenerate at a certain transverse wavenumber $q_{\|}$, and the dispersion curves of ω_1 and ω_2 modes are divided into two parts. However, the right-hand parts cannot be seen due to their moving outside the region explored here (see figure 7(d)). At the same time ω_{2o} and ω_{3o} also disappear. ω_1 and ω_2 are coupled together when they meet each other, while ω_3 is not coupled with ω_1 or ω_2. This indicates that ω_1 and ω_2 possess the same orientation of the polarization and the orientation of the polarization of the ω_3 mode is perpendicular to that of both ω_1 and ω_2. On further decreasing x, both the left-hand part and the right-hand part of ω_1 and ω_2 in the minigap as

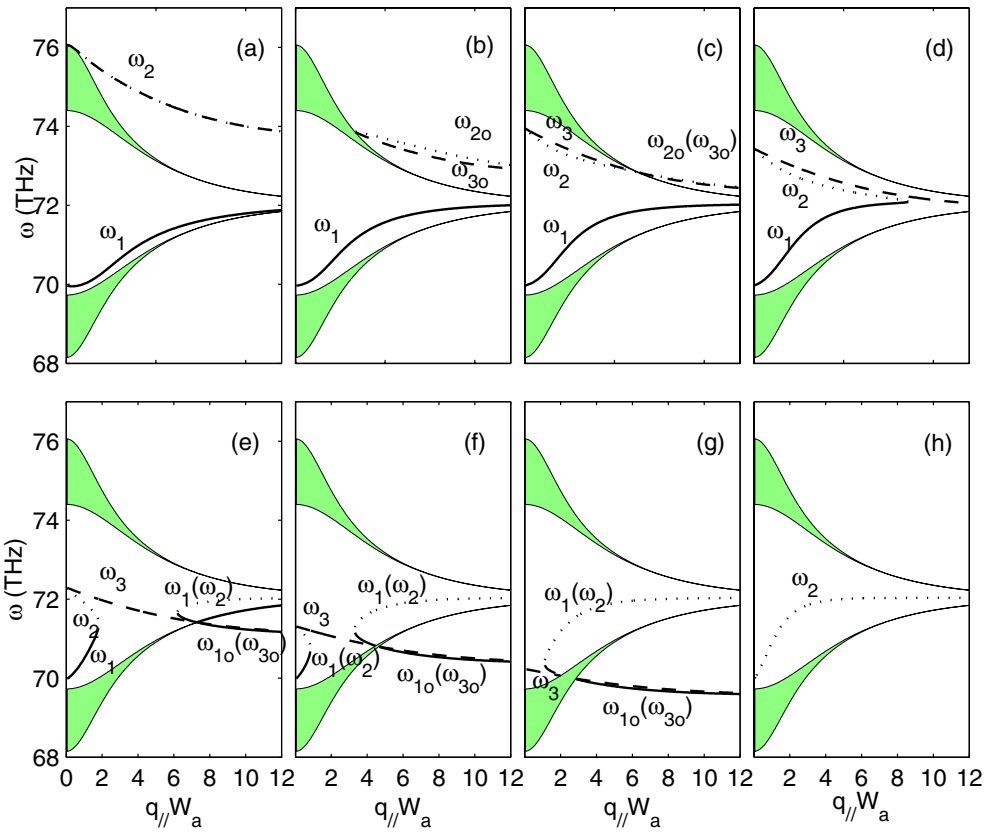

Figure 7. Calculated frequencies of the AlAs-like localized IOPMs as a function of the transverse wavenumber $q_\parallel$ for different concentrations x for the structure: a ternary mixed crystal cap layer $Al_xGa_{1-x}As$ is embedded between a semi-infinite SL and a frequency-independent semi-infinite uniform medium such as SiO_2. (a)–(h) correspond to $x = 1$, 0.7, 0.6, 0.532, 0.4, 0.3, 0.2 and 0.0, respectively. The solid, dotted and dashed curves labelled as ω_1, ω_2 and ω_3, respectively, represent the localized IOPMs lying inside the minigap. ω_{1o}, ω_{2o} and ω_{3o} denote the localized modes lying above and below the bulk bands, respectively. ω_2 (dot–dashed curve) in (a) represents the localized IOPM above the bulk band. The shaded areas indicate the bulk bands of the SL, and the region between the two bulk bands represents the minigap.

well as ω_{1o} and ω_{3o} modes (below the bulk bands) can be clearly seen and they shift towards the left, while ω_3 continues to shift down (see figures 7(e)–(g)). Finally, these modes disappear and only ω_2 survives in the minigap.

We also consider the case of the semi-infinite medium c to be vacuum (dielectric constant $\epsilon = 1$). Similar phenomena can be observed. However, in this case ω_1 in figure 7(a) and ω_2 in figure 7(h) converge to the lower bulk bands when $q_\parallel \to 0$.

In a perfect SL, the allowed minibands originate from the splitting of levels due to the periodicity coupling between two adjacent dielectric layers, while for a semi-infinite SL the periodic coupling is locally broken down around the surface of the semi-infinite SL. The periodicity-broken coupling leads to the appearance of new splitting levels. Some of them may lie within the bulk bands and develop into the delocalized scattering modes, and the rest of them reside in the minigaps or below and above the bulk bands, and become localized IOPMs. For a semi-infinite SL, these localized modes are also called surface optical phonon

modes owing to the fact that they are localized in the vicinity of the surface of the semi-infinite SL. The existence and localization degree of these localized modes depend on the nature and relative thickness of the cap layer and the constituent layers of the SL. When the cap layer is AlAs, there exists one localized IOPM inside the minigap and one above the bulk band; while for a GaAs cap layer, a localized IOPM only exists inside the minigap (see figures 7(a) and (h)). For two coupling semi-infinite SLs with a structural defect layer between them [33], new coupling among two semi-infinite SLs and the defect layer arises. The coupling strengths depend on dielectric response characteristics ϵ_ω (namely, the nature of the material) of the constituent layers, the relative thickness and the stack sequence of the SLs, especially the nature and thickness of the defect layers as intermediate as well as the first adjacent layers of the SL on each side of the defect layer. The existence and the characteristics of the localized IOPMs depend on the coupling strengths. Because the structure presented in [33] is symmetric about the midplane of the defect layer and the dielectric response of the defect layers is the same as that of the constituent layers of the SL, the localized IOPMs always appear in pairs (odd–even parity pair) inside each frequency minigap. However, for the structure considered in figures 5(a) and (h) in this paper, there is only one localized IOPM in each minigap. It seems that the strong coupling among the semi-infinite uniform medium, cap layer and semi-infinite SL causes two localized IOPMs in the minigap to be compressed into one mode. When the defect layers or cap layers are composed of the ternary mixed crystal with different dielectric responses, the coupling will become more complex than that in the structure with the binary crystal defect layer or cap layer due to the two-mode behaviour of the ternary mixed crystals, and the coupling should be different for different structures. Consequently, the localized IOPMs display different features in the structure considered here in comparison to the structures presented in [33] and [34]. Here, it is worth in particular pointing out that for the structures considered in this paper the localized IOPMs exist not only in the minigap, but also below and above the bulk bands, while for the structures presented in [33] and [34] localized IOPMs exist only in the minigap. This should be attributed to the different couplings in different structures. According to these studies, we can conclude that by adjusting the nature and thickness of the cap layers (or defect layers) as well as the constituent layers of the SL, the spectra of the localized IOPMs can be engineered.

In figure 8, we envisage the effects of the thickness of the cap layer on the localized IOPMs for different transverse wavenumbers $q_\parallel$ in the same structure as figure 5. Here, we take $W_a = 20$ nm, $W_b = 5$ nm and $x = 0.3$. Figures 8(a) and (b) correspond to the AlAs-like minigap localized modes for $q_\parallel W_a = 1$ and 4.2, respectively, while figures 8(c) and (d) correspond to the GaAs-like minigap localized modes for $q_\parallel W_a = 1$ and 4.2, respectively. From figure 8(a), it is apparent that there are three branches of localized IOPMs, ω_1, ω_3 and ω_4, existing inside the minigap and their behaviours are sensitive to the thickness of the cap layer. However, there is no localized IOPM surviving outside the bulk bands for arbitrary thickness of the cap layer. With the increase of W_d, the ω_1 branch gradually approaches the lower bulk band, and ω_3 and ω_4 the upper bulk band. For GaAs-like localized IOPMs (see figure 8(c)), similar phenomena are observed except that the values of ω_1, ω_3 and ω_4 branches are just reversed in sequence. For larger transverse wavenumber $q_\parallel$, one can observe seven branches of the localized IOPMs, two (ω_{3o} and ω_{4o}) above and one (ω_{1o}) below the bulk bands, and four (ω_1, ω_2, ω_3 and ω_4) in the minigap. On increasing the thickness of the cap layer, ω_1, ω_2 and ω_3 branches rapidly merge into the bulk bands, while the ω_2 mode survives inside the minigap, and the ω_{1o}, ω_{2o}, and ω_{3o} branches arise from the bulk bands. It is noted that when $W_d > 5$ nm the dispersion curves of the remaining localized modes are almost unchanged (see figures 8(b) and (d)). These results demonstrate that the localized IOPMs are fairly sensitive to the variation of the thickness of the cap layer as well as the transverse wavenumber $q_\parallel$.

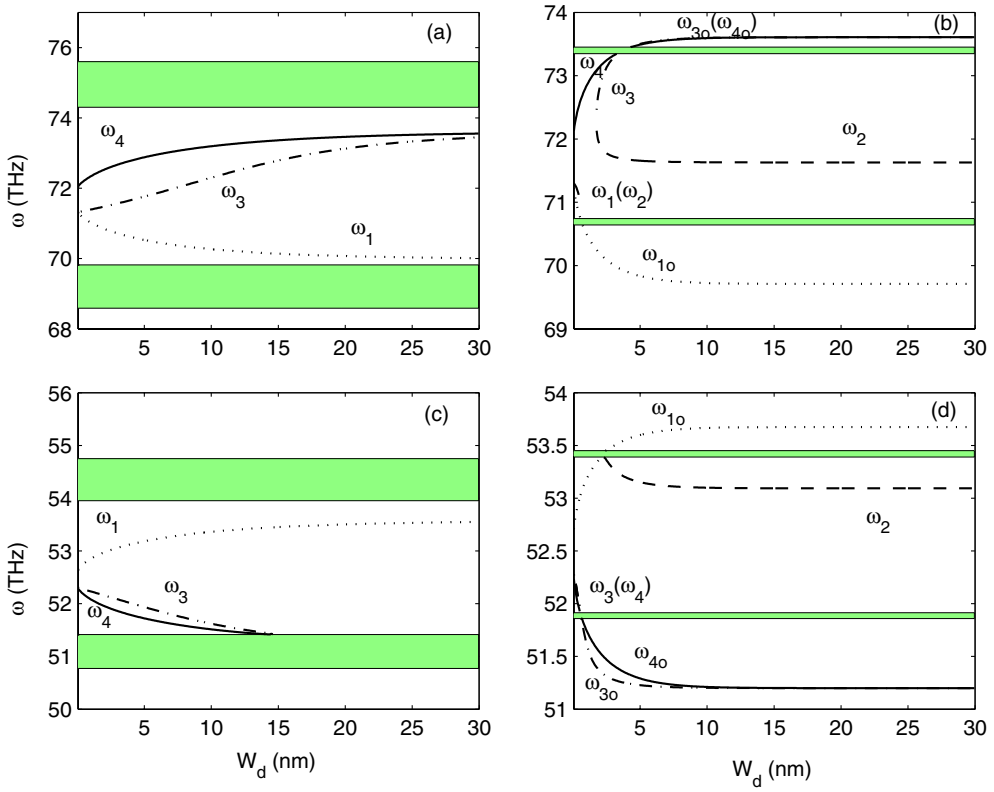

Figure 8. Dependence of frequency of the localized IOPMs on the thickness W_d of the cap layer d: (a) and (b) correspond to the AlAs-like localized IOPMs for $q_\parallel W_a = 1$ and 4.2; (c) and (d) correspond to the GaAs-like localized IOPMs for $q_\parallel W_a = 1$ and 4.2, respectively. Here, we take $W_a = 20$ nm, $W_b = 5$ nm and $x = 0.3$ nm. Explanations for all curves are the same as for figure 5.

Figure 9 reveals the dependence of the localized IOPMs on the thickness W_b of the constituent layer b for different transverse wavenumbers $q_\parallel$. Here, we take $W_a = 20$ nm, $W_d = 3$ nm and $x = 0.3$ nm. Figures 9(a) and (b) correspond to the AlAs-like minigap localized modes for $q_\parallel W_a = 1$ and 4.2, respectively, while figures 9(c) and (d) correspond to the GaAs-like minigap localized modes for $q_\parallel W_a = 1$ and 4.2, respectively. We find that with the increase of the thickness W_b, the bulk bands are gradually broadened, while the minigap is narrowed and finally vanishes at $W_b = W_a = 20$ nm. For small transverse wavenumber $q_\parallel = 1/W_a$, only the ω_1, ω_2 and ω_3 modes appear inside the minigap (see figures 9(a) and (c)). When $q_\parallel = 4.2/W_a$, seven branches of the localized modes appear inside the minigap, below and above the bulk bands, respectively. It is noted that the ω_2, ω_3 and ω_{3o} modes depend on the thickness W_b of the constituent layer b, while, through the range explored, ω_1, ω_{1o}, ω_4 and ω_{4o} remain almost flat (independent of W_b) even for the small values of W_b. This indicates that all the latter modes originate from the two-mode behaviour of the ternary mixed crystal cap layer.

4. Summary

In this paper, we have presented, for the first time to our knowledge, systematic numerical investigations on the localized IOPMs in a semi-infinite SL with a cap layer consisting of a

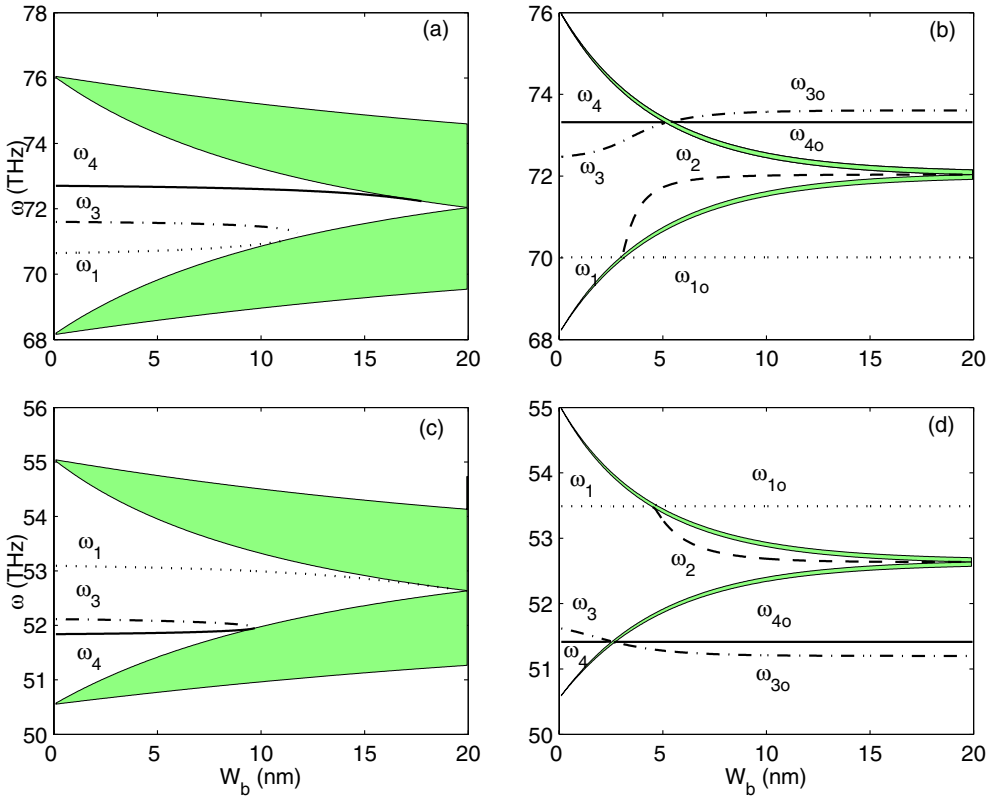

Figure 9. Dependence of frequency of the localized IOPMs on the thickness W_b of the constituent layer b: (a) and (b) correspond to the AlAs-like localized IOPMs for $q_\parallel W_a = 1$ and 4.2; (c) and (d) correspond to the GaAs-like localized IOPMs for $q_\parallel W_a = 1$ and 4.2, respectively. Here, we take $W_a = 20$ nm, $W_d = 3$ nm and $x = 0.3$ nm. Explanations for all curves are the same as for figure 5.

ternary mixed crystal attached to a semi-infinite uniform dielectric medium. The obtained results show that the localized IOPMs are fairly sensitive to the nature and the thickness of the cap layer, and the kind of semi-infinite uniform dielectric medium. The introduction of two-mode behaviour of the ternary mixed crystal in the cap layer or the semi-infinite uniform dielectric medium leads to rich and varied localized mode spectra which display interesting characteristics such as that several localized modes exist inside the minigap, above the bulk band or below the bulk band, respectively; two modes with the same orientation of the polarization can be strongly coupled together when they meet each other and all the peaks and valleys of the modulus of the macroscopic electrostatic potential of the localized IOPMs are located at the interfaces etc. A detailed comparison of the localized IOPMs in several structures has been addressed. We also present a qualitative analysis of the origination of the localized IOPMs. We suggest that Raman scattering may be utilized to probe the localized IOPMs predicted here. It is expected that the localized IOPMs can be artificially tailored by adjusting the physical and geometrical parameters of the proposed micro-structures.

Acknowledgment

This work was supported by the National Natural Science Foundation of China, the National High Technology Research and Development Program of China (Grant No 2002AA311153) the Ministry of Education of China, and the China Postdoctoral Science Foundation.

References

[1] Camley R E and Mills D L 1984 *Phys. Rev.* B **29** 1695
[2] Yip Sung-kit and Chang Yia-Chung 1984 *Phys. Rev.* B **30** 7037
[3] Lambin Ph, Vigneron J P and Lucas A A 1985 *Phys. Rev.* B **32** 8203
[4] Huang K and Zhu B F 1988 *Phys. Rev.* B **38** 2183
Huang K and Zhu B F 1988 *Phys. Rev.* B **38** 13377
[5] Dereux A, Vigneron J-P, Lambin P and Lucas A A 1988 *Phys. Rev.* B **38** 5438
[6] Ridley B K 1989 *Phys. Rev.* B **39** 5282
[7] Rudin S and Reinecke T L 1990 *Phys. Rev.* B **41** 7713
[8] Nash K J 1992 *Phys. Rev.* B **46** 7723
[9] Yu Se Gi, Kim K W, Stroscio M A, Iafrate G J, Sun J-P and Haddad G I 1997 *J. Appl. Phys.* **82** 3363
[10] Velasco V R and Garcia-Moliner F 1997 *Surf. Sci. Rep.* **28** 123
[11] Merlin R, Colvard C, Klein M V, Morkoo H, Cho A Y and Gossard A G 1980 *Appl. Phys. Lett.* **36** 43
[12] Sood A K, Menendez J, Cardona M and Ploog K 1985 *Phys. Rev. Lett.* **54** 2115
[13] Colvard C, Gaut T A, Klein M V, Merlin R, Fischer R, Morkoc H and Gossard A C 1985 *Phys. Rev.* B **31** 2080
[14] Lambin Ph, Vigneron J P, Lucas A A, Thirty P A, Liehr M, Pireaux J J and Caudano R 1986 *Phys. Rev. Lett.* **56** 1842
[15] Ambrazevicius A, Cardona M, Merlin R and Ploog K 1988 *Solid State Commun.* **65** 1035
[16] Fainstein A, Etchegoin P, Chamberlain M P, Cardona M, Totemeyer K and Ebert K 1995 *Phys. Rev.* B **51** 14448
[17] Shields A J, Chamberlain M P, Cardona M and Eberl K 1995 *Phys. Rev.* B **51** 17728
[18] Zucker J E, Pinczuk A, Chemla D S, Gossard A and Wiegmann W 1984 *Phys. Rev. Lett.* **53** 1280
[19] Mori N and Ando T 1989 *Phys. Rev.* B **40** 6175
[20] Duan W, Zhu Jia-Lin and Gu Bing-Lin 1993 *J. Phys.: Condens. Matter* **5** 2859
Duan W, Zhu Jia-Lin and Gu Bing-Lin 1994 *Phys. Rev.* B **49** 14403
[21] Gu Bing-Lin, Duan Wenhui, Xiong Shiying and Guo Youjiang 1996 *Phys. Rev.* B **54** 16983
[22] Zheng Ruisheng and Matsuura Mitsuru 1999 *Phys. Rev.* B **60** 4937
[23] Kim Dae Kwan, Roblin P, Soh Kwang-Sup and Kim Chul Koo 2002 *Phys. Rev.* B **65** 115328
[24] Johnson B L, Weiler J T and Camley R E 1985 *Phys. Rev.* B **32** 6544
[25] Nkoma J S 1987 *Surf. Sci.* **191** 595
[26] Liu Wen-ming, Eliasson G and Quinn J J 1985 *Solid State Commun.* **55** 533
[27] Streight S R and Mills D L 1987 *Phys. Rev.* B **35** 6337
[28] Tsuruoka T, Uehara Y and Ushioda S 1994 *Phys. Rev.* B **49** 4745
[29] Mendialdua J, Rodriguez A, More M, Akjouj A and Dobrzynski L 1994 *Phys. Rev.* B **50** 14605
[30] Bah M L, Akjouj A, El Boudouti E H, Djafari-Rouhani B and Dobrzynski L 1996 *J. Phys.: Condens. Matter* **8** 4171
[31] Lahlaouti M L H, Akjouj A, Djafari-Rouhani B and Dobrzynski L 2000 *Phys. Rev.* B **61** 2059
[32] Deych L I, Yamilov A and Lisyansky A A 2001 *Phys. Rev.* B **64** 075321
[33] Chen Ke-Qiu, Wang Xue-Hua and Gu Ben-Yuan 2000 *Phys. Rev.* B **62** 9919
[34] Chen Ke-Qiu, Wang Xue-Hua and Gu Ben-Yuan 2002 *Phys. Rev.* B **65** 153305
[35] Chang I F and Mitra S S 1971 *Adv. Phys.* **20** 359
[36] Adachi S 1985 *J. Appl. Phys.* **58** R1
[37] Tamura S and Wolfe J P 1987 *Phys. Rev.* B **35** 2528
[38] Wang Xue-Hua, Chen Ke-Qiu and Gu Ben-Yuan 2002 *J. Appl. Phys.* **92** 5113